Blue Light Excited Broadband NIR-II-emitting $Li_2ZnSn_3O_8:Cr^{3+},Ni^{2+}$ Phosphor for Multifunctional Optical Applications

Zhexuan Gao[a], Yi Zhang[a], Yinyan Li[a], Shilong Zhao[a], Peng Zhang[a], Xiaolong Dong[b], Degang Deng*[a], Shiqing Xu*[a]

[a] *Key Laboratory of Rare Earth Optoelectronic Materials and Devices of Zhejiang Province, Institute of Optoelectronic Materials and Devices, China Jiliang University, Hangzhou 310018, China*

[b] *Fujian Institute of Metrology, Fuzhou,350003, China*

Supporting information

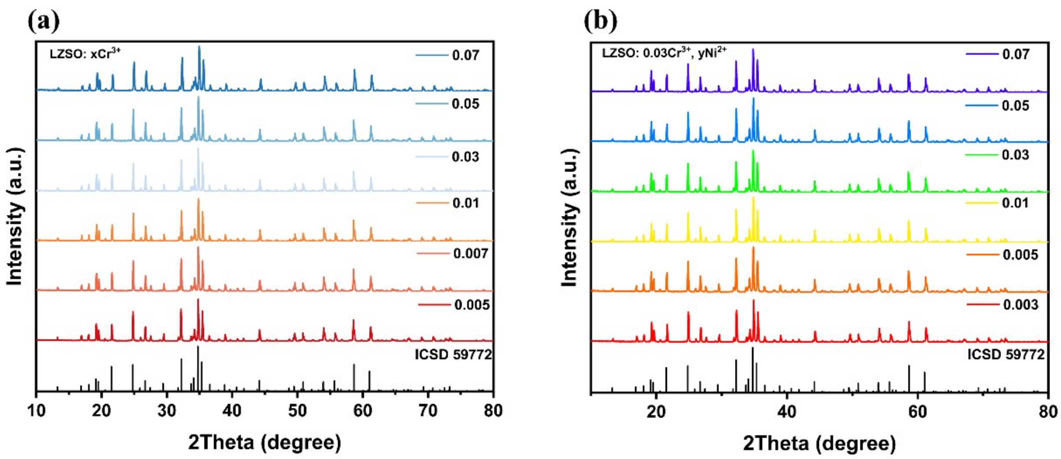

Figure S1. Powder XRD patterns of a) LZSO:$y$$Cr^{3+}$, and b) LZSO:0.03$Cr^{3+}$,$y$$Ni^{2+}$ samples (x, y = 0.003-0.07). The corresponding standard PDF card data of LZSO (ICSD 59772) is given as a reference.

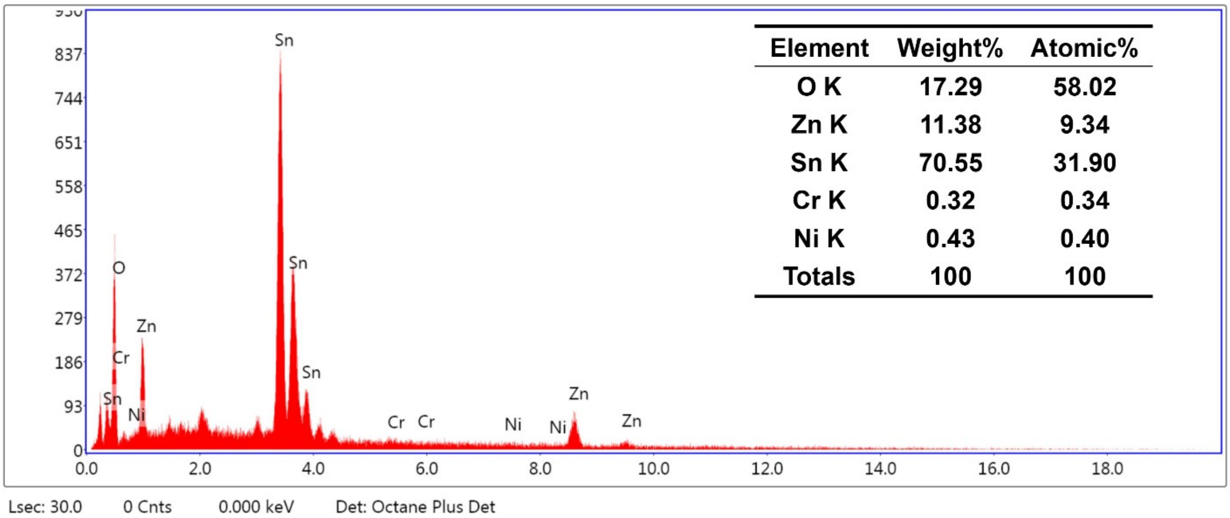

Figure S2. The EDS spectrum of LZSO:$0.03Cr^{3+}$,$0.03Ni^{2+}$ phosphor.

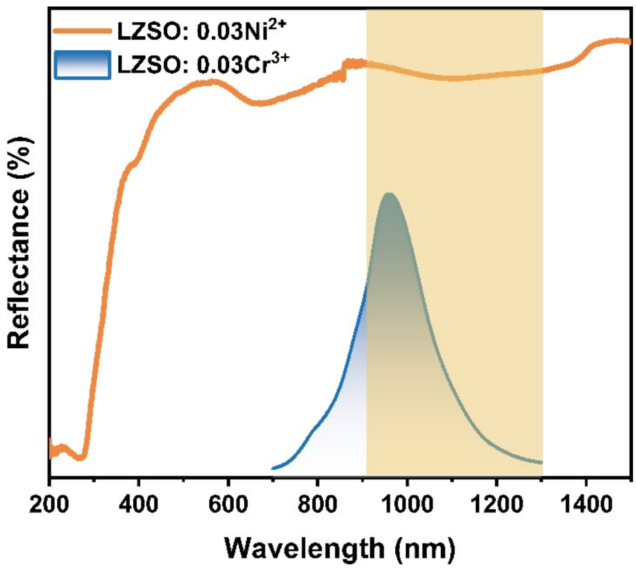

Figure S3. The overlap between the PL of LZSO:Cr^{3+} and PLE of LZSO:Ni^{2+}.

The Tanabe−Sugano energy level diagram can be used to represent the split of the 3d8 energy levels of Ni^{2+} in the octahedral field when Ni^{2+} ($3d^8$) ions are located in the octahedral coordination field, and the crystal field strength of Ni^{2+} in the octahedral can be described using the Tanabe−Sugano theory, and the crystal field strength Dq and Racah parameter B can be obtained according to the following equation:[(1)]

$$D_q = \frac{\nu_1}{10} \quad (1)$$

$$B = \frac{(\nu_3 - 2\nu_1)\cdot(\nu_3 - \nu_1)}{3(5\nu_3 - 9\nu_1)} \quad (2)$$

In the equations, v_3 and v_1 correspond to 400 nm [$^3A_{2g}(F) \rightarrow {}^3T_{1g}(P)$, 25000cm^{-1}], and 1100 nm [$^3A_{2g}(F) \rightarrow {}^3T_{2g}(F)$, 9090.9 cm^{-1}], respectively. Therefore, *Dq* is 909.09 cm^{-1}, *B* is 837.32 cm^{-1} and *Dq*/*B* is 1.09, respectively.

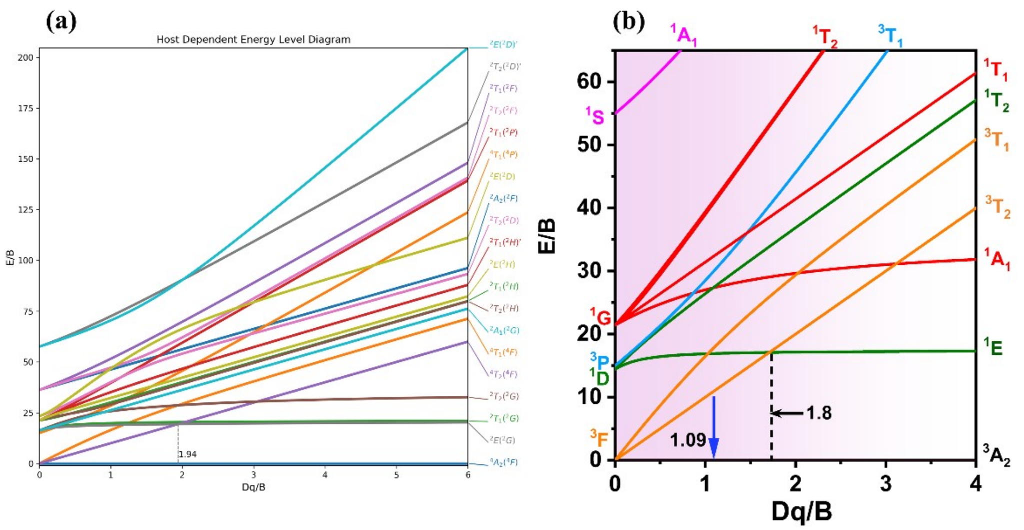

Figure S4. Tanabe-Sugano diagram for a) Cr^{3+} and b) Ni^{2+} ion in octahedral coordination.

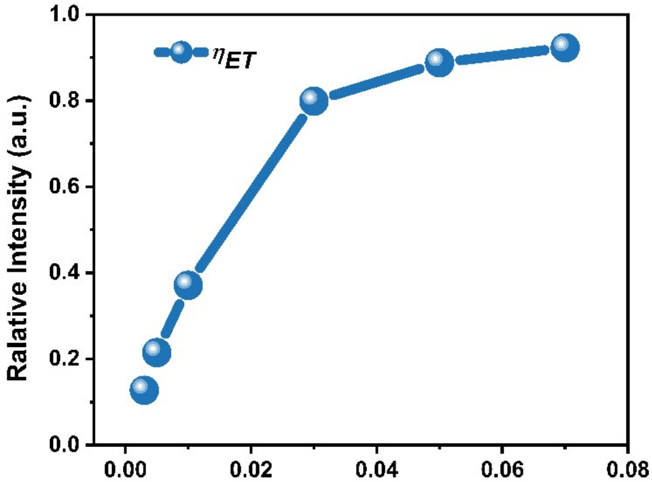

Figure S5 The ET efficiency based on the Intensity of Cr^{3+} concentration in LZSO:0.03Cr^{3+},$y$$Ni^{2+}$ system.

IQE is the ratio of the number of emitted photons to the number of absorbed photons, EQE is the ratio of the number of emitted photons to the number of total photons excited by the light source, and absorption efficiency (αAbs) is the proportion of the number of photons absorbed by the sample and the number of total photons excited by the light source. The relationship among IQE, EQE and αAbs can be expressed by the following equations:[(2)]

$$IQE = \frac{\int L_S}{\int E_R - \int E_S} \tag{3}$$

$$AE = \frac{\int E_R - \int E_S}{\int E_R} \tag{4}$$

$$EQE = AE \times IQE = \frac{\int L_S}{\int E_R} \tag{5}$$

where E_S stands for the spectrum used for exciting the phosphor, L_S represents the emission spectrum of the phosphor, and E_R is the spectrum of excitation light without phosphor in the sphere. Taking into account the 2.13% unmeasured portion. Hence, the IQE, *AE*, and *EQE* of LZSO:0.03Cr^{3+},0.03Ni^{2+} are 43.31%, 42.11%, and 18.24%.

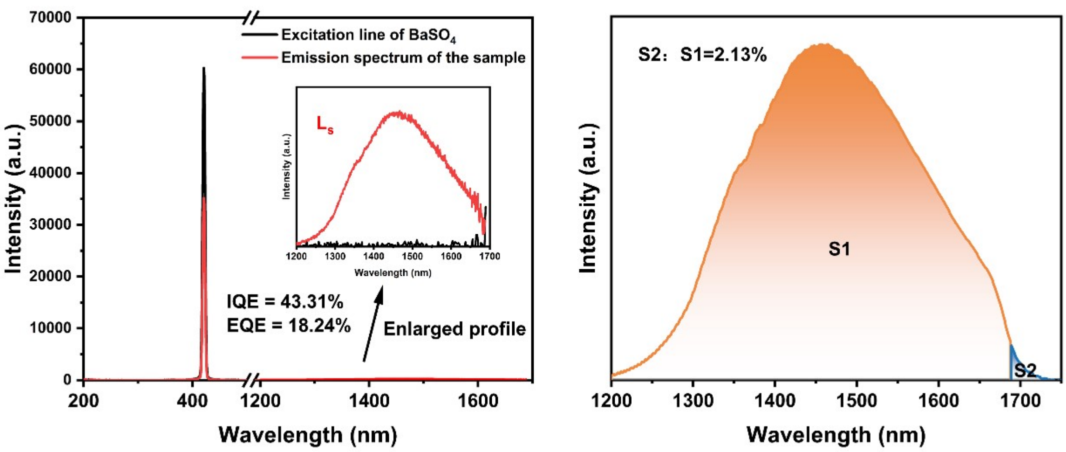

Figure S6 IQE and EQE of LZSO:0.03Cr^{3+},0.03Ni^{2+}.

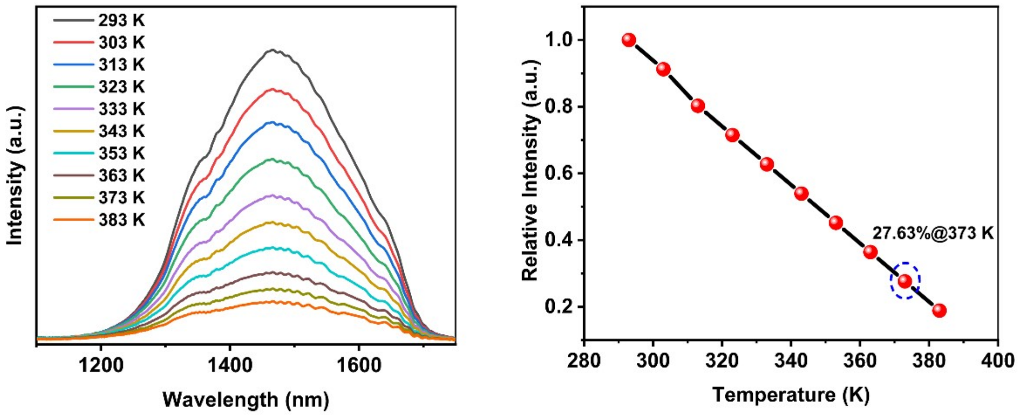

Figure S7 Temperature-dependent emission spectra and relative intensity of LZSO: $0.03Ni^{2+}$.

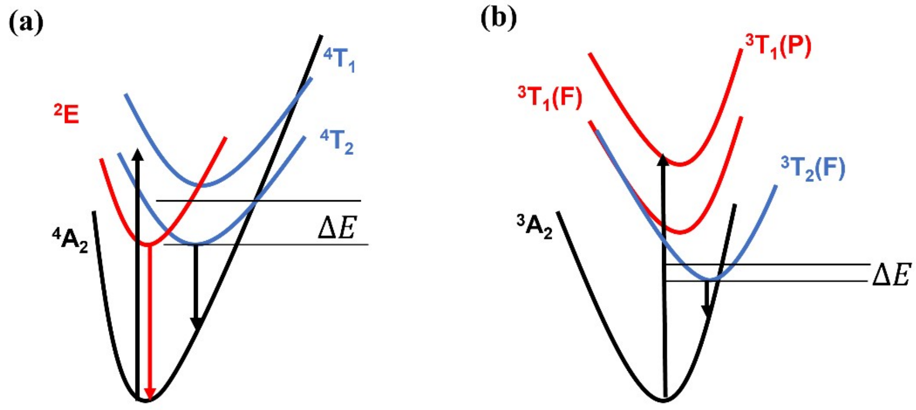

Figure S8. Configuration coordinate diagram of Cr^{3+} and Ni^{2+} illustrating the thermal quenching.

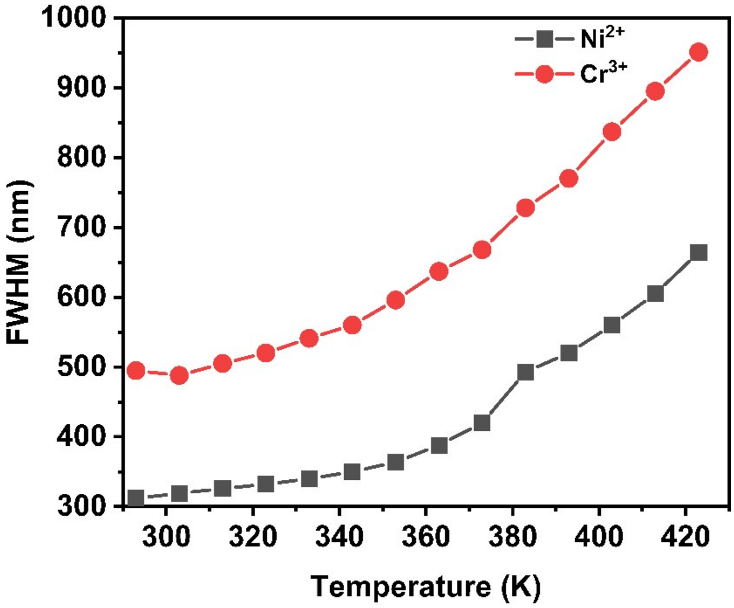

Figure S9. FWHM of LZSO:0.03Cr^{3+},0.03Ni^{2+}.

Table S1. Refined results of the LZSO sample

formula	LZSO
radiation type; λ (Å)	X-ray; 1.5406
2θ (degrees)	10-80
temperature (°C)	20
space group	Cmc21
a (Å)	18.2355
b (Å)	10.5209
c (Å)	9.8906
$\alpha = \beta = \gamma$(degrees)	90
V (Å^3)	1897.558
profile R-factor, R_p	5.85
weighted profile R-factor, R_{wp}	9.28
χ^2	1.584

Table S2. Refined atomic positions of the LZSO sample

atom	occ.	x	y	z	uiso	site
Sn1	1	0.0875	0.0715	0	0.01369	8b
Sn2	1	0.0856	0.5927	0.001	0.01442	8b
Sn3	1	0.1726	0.334	0.004	0.01194	8b
Li1	1	0.249	0.082	0.007	0.012	8b
Li2	1	0	0.836	0.01	0.01362	4a
Li3	1	0	0.032	0.293	0.01186	4a
Li4	1	0.182	0.481	0.279	0.0142	8b
Zn1	1	0	0.331	0.19	0.01362	4a
Zn2	1	0.167	0.831	0.193	0.01186	8b
Sn4	1	1	0.669	0.283	0.01819	4a
Sn5	1	0.168	0.168	0.281	0.01548	8b
O1	1	0	0.159	-0.108	0.01588	4a
O2	1	0.0834	-0.078	-0.121	0.01617	8b
O3	1	0	0.664	-0.105	0.01663	4a
O4	1	0.0825	0.42	-0.111	0.0132	8b
O5	1	0.249	0.415	-0.119	0.01195	8b
O6	1	0.1651	0.67	-0.108	0.01728	8b
O7	1	0.165	0.171	-0.103	0.01353	8b
O8	1	0	0.007	0.108	0.01439	4a
O9	1	0	0.52	0.135	0.01172	4a
O10	1	0.0918	0.241	0.128	0.01439	8b
O11	1	0.0773	0.738	0.141	0.01671	8b
O12	1	0.1648	0.014	0.139	0.01624	8b
O13	1	0.2389	0.251	0.147	0.01444	8b
O14	1	0.1653	0.5	0.1	0.01319	8b

Table S3. The optical performance comparison of LZSO:0.03Cr^{3+},0.03Ni^{2+} and previously reported NIR-II phosphors

Phosphors	Excitaion (nm)	*FWHM (nm)*	*Emission range (nm)*	*IQE (%)*	*EQE (%)*	*Ref*
Ba_2MgWO_6:Ni^{2+}	365	255	1200−2000	16.67	--	(3)
$SrTiO_3$:Ni^{2+}	375	192	1100–1600	7.4	--	(4)
$MgTiO_3$:Ni^{2+}	450	120	1500–2000	3.1	--	(4)
$CaTiO_3$:Ni^{2+}	375	212	1150–1600	4.3	--	(5)
$MgAl_2O_4$:Ni^{2+}	365	237	1100–1600	--	--	(6)
$ZnGa_2O_4$:Ni^{2+}	365	--	1100–1600	--	--	(7)
$Y_3Al_2Ga_3O_{12}$:Ni^{2+}	400	300	1200–1650	54	8.2	(1)
$Mg_3Ga_2GeO_8$:Ni^{2+}	395	300	1100–1700	36.7	7.3	(8)
$Mg_2Ta_4O_9$:Ni^{2+}	404	218	1100–1700	64	11.2	(9)
MgO:Ni^{2+}	405	204	1100–1700	--	--	(10)
LZSO:0.03Cr^{3+},0.03Ni^{2+}	426	300	1100–1750	43	18	This work

Reference

1. Yuan L, Jin Y, Wu H, Deng K, Qu B, Chen L, et al. Ni^{2+}-Doped Garnet Solid-Solution Phosphor-Converted Broadband Shortwave Infrared Light-Emitting Diodes toward Spectroscopy Application, *ACS Appl. Mater. Interfaces*, 2022, **14**, 4265-4275.
2. Chen S, Lin J, Han M, Li J, Zhang Q, Chen Y, et al. Broadband near-infrared emitting Cr^{3+}-activated $InGaO_3(ZnO)_4$ phosphor and its application in pc-LEDs. *Mater. Res. Bull.*, 2023, **164**, 112280.
3. Lu X, Gao Y, Chen J, Tan M, Qiu J. Long-Wavelength Near-Infrared Divalent Nickel-Activated Double-Perovskite Ba_2MgWO_6 Phosphor as Imaging for Human Fingers, *ACS Appl. Mater. Interfaces*, 2023, **15**, 39472-39479.
4. Gao Y, Wang B, Liu L, Shinozaki K. Near-infrared engineering for broad-band wavelength-tunable in biological window of NIR-II and -III: A solid solution phosphor of $Sr_{1-x}Ca_xTiO_3$:Ni^{2+}, *J. Lumin.*, 2021, **238**, 118235.
5. Matuszewska C, Marciniak L. The influence of host material on NIR II and NIR III emitting Ni^{2+}-based luminescent thermometers in $ATiO_3$: Ni^{2+} (A = Sr, Ca, Mg, Ba) nanocrystals, *J. Lumin.*, 2020, **223**, 117221.
6. Deng Y, Gao Y, Zhu F, Zhu B, Huang L, Qiu J. Sol-gel combustion synthesis and near-infrared luminescence of Ni^{2+}-doped $MgAl_2O_4$ spinel phosphor, *Ceram. Int.*, 2024, **50**, 12319-12325.
7. Jin M, Li F, Xiahou J, Zhu L, Zhu Q, Li J-G. A new persistent luminescence phosphor of $ZnGa_2O_4$:Ni^{2+} for the second near-infrared transparency window, *J. Alloy. Compd*, 2023, **931**, 167491.
8. Wang C, Lin J, Zhang X, Dong H, Wen M, Zhao S, et al. Efficient ultra-broadband NIR-II emission achieved by multi-site occupancy in $Mg_3Ga_2GeO_8$: Ni^{2+} phosphor, *J. Alloy. Compd.*, 2023, **942**, 168893.
9. Li J, Wang C, Niu Y, Wang Y, Wu F, Qi z, et al. Efficient broad-band NIR-II emitting phosphor $Mg_4Ta_2O_9$: Ni^{2+} with satisfactory thermal stability of luminescence, *Ceram. Int.*, 2024, **50**, 18647-18654.
10. Liu B-M, Gu S-M, Huang L, Zhou R-F, Zhou Z, Ma C-G, et al. Ultra-broadband and high-efficiency phosphors to brighten NIR-II light source applications, *Cell Rep. Phys. Sci*, 2022, **3**, 101078.